Journal of the Taiwan Institute of Chemical Engineers 126 (2021) 297–306

Contents lists available at ScienceDirect

Journal of the Taiwan Institute of Chemical Engineers

journal homepage: www.elsevier.com/locate/jtice

Reaction-inhibited interfacial coating between PEDOT:PSS sensing membrane and ITO electrode for highly-reliable piezoresistive pressure sensing applications

Jer-Chyi Wang[a,b,c,d,*], Rajat Subhra Karmakar[a], Ting-Han Lin[e], Ming-Chung Wu[b,e,f,*], Kuo-Hsuan Chang[g,h,*]

[a] Department of Electronic Engineering, Chang Gung University, Guishan Dist. 33302, Taoyuan, Taiwan
[b] Green Technology Research Center, Chang Gung University, Guishan Dist. 33302, Taoyuan, Taiwan
[c] Department of Neurosurgery, Chang Gung Memorial Hospital, Linkou, Guishan Dist. 33305, Taoyuan, Taiwan
[d] Department of Electronic Engineering, Ming Chi University of Technology, Taishan Dist. 24301, New Taipei City, Taiwan
[e] Department of Chemical and Materials Engineering, Chang Gung University, Guishan Dist. 33302, Taoyuan, Taiwan
[f] Division of Neonatology, Department of Pediatrics, Chang Gung Memorial Hospital, Linkou, Guishan Dist. 33305, Taoyuan, Taiwan
[g] Department of Neurology, Chang Gung Memorial Hospital, Linkou, Guishan Dist. 33305, Taoyuan, Taiwan
[h] School of Medicine, Chang Gung University, Guishan Dist. 33302, Taoyuan, Taiwan

ARTICLE INFO

Article History:
Received 29 March 2021
Revised 13 June 2021
Accepted 4 July 2021
Available online 15 July 2021

Keywords:
Poly(3,4-ethylenedioxythiophene): poly-(styrenesulfonate) (PEDOT:PSS), Indium tin oxide (ITO), Piezoresistive pressure sensor, Interfacial coating, Polyethylene terephthalate (PET), Package

ABSTRACT

Background: Poly(3,4-ethylenedioxythiophene):poly-(styrenesulfonate) (PEDOT:PSS) is a promising conductive polymer for the flexible piezoresistive pressure sensor. However, intrinsic hydrophilicity is detrimental to its structural stability under moisture. The present study aims to enhance piezoresistive pressure sensors' stability to achieve the highly-reliable electronic device applications.
Method: ITO/PEDOT:PSS/ITO piezoresistive pressure sensors with an interdigitated electrode (IDE) structure and different metallic interfacial layers were fabricated. Au layer was introduced between PEDOT:PSS sensing membrane and indium tin oxide (ITO) electrode as a reaction-inhibited interfacial coating of piezoresistive pressure sensors.
Significant findings: After a measurement time interval of 6 months, the interface reaction suppressed significantly, resulting in low sensitivity deviation (9.22%) and improved durability (400 cycles). The devices are completely sealed using polyethylene terephthalate packaging, avoiding humidity absorption in PEDOT:PSS films successfully. The packaged ITO/PEDOT:PSS/ITO piezoresistive pressure sensors with a double-sided 10-nm-thick Au interfacial layer is a promising candidate for use in highly reliable pressure sensing applications.

1. Introduction

In recent technological advancements, flexible electronic devices have garnered significant interest due to their advantages over conventional semiconductor devices, such as extraordinary flexibility, bendability and stretchability [1–3]. This technology has emerged from alternative low cost and mass production methods; for example, ink-jet printing and roll-to-roll imprinting [4,5]. Among the flexible devices, pressure sensors have received considerable attention in the scientific and industrial communities because of their extensive usage in various fields [6–9]. Piezoresistive, piezoelectric, and capacitive pressure sensors are the three foremost technologies in the pressure-sensing industry, where piezoresistive sensors with the highest sensitivity and lowest cost are extensively employed [10–12]. Poly(3,4-ethylenedioxythiophene):poly-(styrenesulfonate) (PEDOT:PSS), which is a conductive polymer with high transparency, high electrochemical and thermal stability, and favorable optical properties, is an excellent material for flexible piezoresistive pressure sensing [13–20]. PEDOT is a conductive polymer based on the monomer 3,4-ethylenedioxythiophene (EDOT) and is blended with polystyrene sulphonate (PSS) during polymerization to form PEDOT:PSS for the balance of cationic charges and the allowance of dispersion in water; hence, it is suitable for manufacturing via spin-coating, drop-casting and printing methods [13,16,17]. In addition to sensing materials, a suitable electrode material that can withstand the bending and stretching of flexible pressure sensors must be selected. Indium tin oxide (ITO), which exhibits good optical transparency and superb electrical conductivity, has been proposed as one of the most promising electrode materials for flexible electronic devices such as photovoltaic devices and light-emitting diodes (LEDs) [21–23]. Its high

* Corresponding authors.
E-mail addresses: jcwang@mail.cgu.edu.tw (J.-C. Wang), mingchungwu@cgu.edu.tw (M.-C. Wu), gophy5128@cgmh.org.tw (K.-H. Chang).

https://doi.org/10.1016/j.jtice.2021.07.004
1876-1070/

electron density of 10^{21} cm^{-3} in the conduction band, low-temperature manufacturing on flexible substrates, and sufficient stability in aqueous solutions render it suitable for electrochemical applications [24,25].

Unfortunately, environmental stability is a major concern for PEDOT:PSS films. A substantial volume of the films is occupied by long PSS chains, resulting in low conductivity and poor device performance because of the disruption of PEDOT chain arrangement [26]. Furthermore, in a humid environment, PEDOT:PSS films are extremely hygroscopic because PSS chains can absorb water for unintentional swelling, which is detrimental to their structural stability [27,28]. Lin et al. reported that the post-deposition annealing of PEDOT:PSS films in air is generally unstable due to rapid water uptake [29], implying that the delamination of PEDOT:PSS films is caused by a combination of thermomechanical, hygroscopic, and voltage-induced stresses [30–34]. To improve the aqueous stability of PSS in water, chemical cross-linkers have been typically employed. However, both electronic and ionic mobilities of PEDOT:PSS films will be seriously degraded owing to the interference with interchain charge transport by the chemical cross-linking-induced densification [26,35–38]. For the application of PEDOT:PSS films in organic LEDs and organic solar cells, ITO electrodes have been employed and was discovered to be etched by PEDOT:PSS solution because of the strongly acidic nature of PSS, causing the diffusion of indium ions into PEDOT:PSS films and weakening the stability of the PEDOT:PSS and ITO interface [39–43]. Although the reactions between PEDOT:PSS and ITO could be blocked via a deposition of an interfacial self-assembled monolayer (SAM) of alkylsiloxanes, the toxic and high-resistance nature of SAM layers limits their utilizations [41]. Currently, pressure sensors with a long lifetime under electromechanical testing are essential for scientific and industrial applications. Nevertheless, studies pertaining to the enhancement of the time-dependent reliability of PEDOT:PSS and ITO interfaces by metallic interfacial coatings and their applications in piezoresistive pressure sensors have not been conducted. In this study, reaction-inhibited interfacial coatings between PEDOT:PSS sensing membranes and ITO electrodes were demonstrated for the first time. To acquire a robust ITO/PEDOT:PSS/ITO piezoresistive pressure sensor, the types and thicknesses of the metallic interfacial layers were adjusted. The surface morphology, surface potential, and composition of PEDOT:PSS films on ITO layers were analyzed via material analysis, and the piezoresistive pressure sensing properties of the devices were characterized based on resistance *vs*. pressure (R–P) curves. To further enhance the stability, a complete sealing was implemented into the piezoresistive pressure sensors via polyethylene terephthalate (PET) packaging to eliminate the absorption of humidity in a normal environment. Compared with samples without any interfacial layer, the packaged ITO/PEDOT:PSS/ITO piezoresistive pressure sensors with metallic interfacial coatings demonstrated a low sensitivity deviation and stable cycling testing, which were correlated with the reduction in bright spots in field-emission scanning electron microscopy (FE-SEM) images, In–O–H bonds in the X-ray electron microscopy (XPS) spectra, and Raman shift. No dissolution of In_2O_3 from ITO layers in acidic PEDOT:PSS copolymers was achieved using a double-sided Au interfacial coating; hence, a double-sided Au interfacial coating is suitable for future flexible electronics and pressure sensing applications.

2. Experimental

2.1. Sample preparation

ITO/PEDOT:PSS/ITO piezoresistive pressure sensors with an interdigitated electrode (IDE) structure and different metallic interfacial layers were fabricated. The IDE structure comprises two parts, *i.e.*, parts I and II, where part I is a patterned ITO electrode on a PET substrate, and part II is an ITO/PET substrate with a spin-coated PEDOT:PSS film. In this study, a 0.35-μm-thick ITO film covered on a 188-μm-thick flexible PET substrate was obtained from Sigma–Aldrich Co. (St. Louis, USA). The ITO/PET substrates were cleaned in an acetone, methanol, and deionized (DI) water bath for 3 min. Subsequently, a thin Al interfacial layer with a thickness of 5 nm and Au interfacial layers with thicknesses of 5, 10, and 20 nm were directly deposited on ITO/PET substrates using a thermal evaporator (Fig. 1a,b and e,f), which has been used to improve the interface quality between the ITO anode and the organic layer in organic LEDs for better electrical performance [44]. The operating pressure was 10^{-6} Torr with pure Al and Au bullets (99.999% purity). For part I, the IDE pattern was transferred via conventional photolithography (Fig. 1c). The ITO/PET substrates were coated with a positive photoresist (AZ-6112, Merck KGaA, Darmstadt, Germany) and exposed to ultraviolet light for 6 s through a photomask. Then, the photoresist was developed (AZ-300, Merck KGaA, Darmstadt, Germany), and a solution comprising HCl, HNO_3, and H_2O with a volumetric mix ratio of 50:3:50 was used to etch the ITO. For the samples with an Au interfacial layer in part I, the Au-401B etchant solution provided by Chemleader Corp., Taiwan was used to etch the Au film prior to etching the ITO. The top-view image of the well-defined patterned electrode was analyzed using an optical microscope, as shown in Fig. 1d. For part II, the ITO/PET, Al/ITO/PET, and Au/ITO/PET substrates were cleaned with acetone and DI water bath. To render the surface hydrophilic for the spin-coating of PEDOT:PSS films, the substrates were treated by an O_2 plasma for 10 min. Thus, some polar groups on the top of the substrates were created. The aqueous solution with a PEDOT:PSS concentration of 1.6 wt% and a resistivity of 785 Ω•cm (Clevios P VP AI 4083, Heraeus Holding GmbH, Germany) was used to form the PEDOT:PSS sensing membrane on the O_2-plasma-treated surfaces. The substrates were vacuumed on a spin-coater and a specific amount of PEDOT:PSS solution was dropped on the substrates. To make the solution uniformly distributed over the substrates, a lower spin-coating speed of 300 rpm (revolutions per minute) for 5 s was performed and then a higher spin-coating speed of 500 rpm for 10 s was used to achieve the desired PEDOT:PSS film thickness. Then, all samples were subjected to the hot plate and baked at 120 °C for 20 min to evaporate excess water, as shown in Fig. 1g. The thickness of the fabricated PEDOT:PSS sensing membranes was approximately 1.9 μm, which was confirmed using an alpha-step surface profiler (DektakXT Stylus profiler, Bruker, Massachusetts, USA). Finally, the ITO/PET substrate with a spin-coated PEDOT:PSS film (part II) was overturned and put on the patterned ITO electrode of part I to form a sandwich structure for piezoresistive pressure sensing (Fig. 1h) and the devices were packaged using a commercial PET to avoid humidity absorption. The thickness of the PET packaging film was approximately 60 μm with glue at one side of the film. Two pieces of the PET packaging films were prepared and placed at the top and the bottom of the sandwich devices separately and then sealed together. Fig. 1i shows a real-time image of the packaged ITO/PEDOT:PSS/ITO piezoresistive pressure sensing device with a double-sided 10-nm-thick Au interfacial layer. The sensing area was approximately 2.56 cm^2. In addition, the cross-sectional schematics of the devices with and without single-sided and double-sided metallic interfacial layers are illustrated in Fig. 1j–m.

2.2. Characterization of materials and devices

The key focus of this study is the time-dependent reliability evaluation of ITO/PEDOT:PSS/ITO piezoresistive pressure sensors with different metallic interfacial layers. Hence, all samples were stored under atmospheric conditions for 6 months and investigated after a particular interval. Samples investigated immediately after fabrication were denoted as Day 0, whereas those investigated the day after fabrication and after 2 days, 1 week, 2 weeks, 3 weeks, 1 month, 2

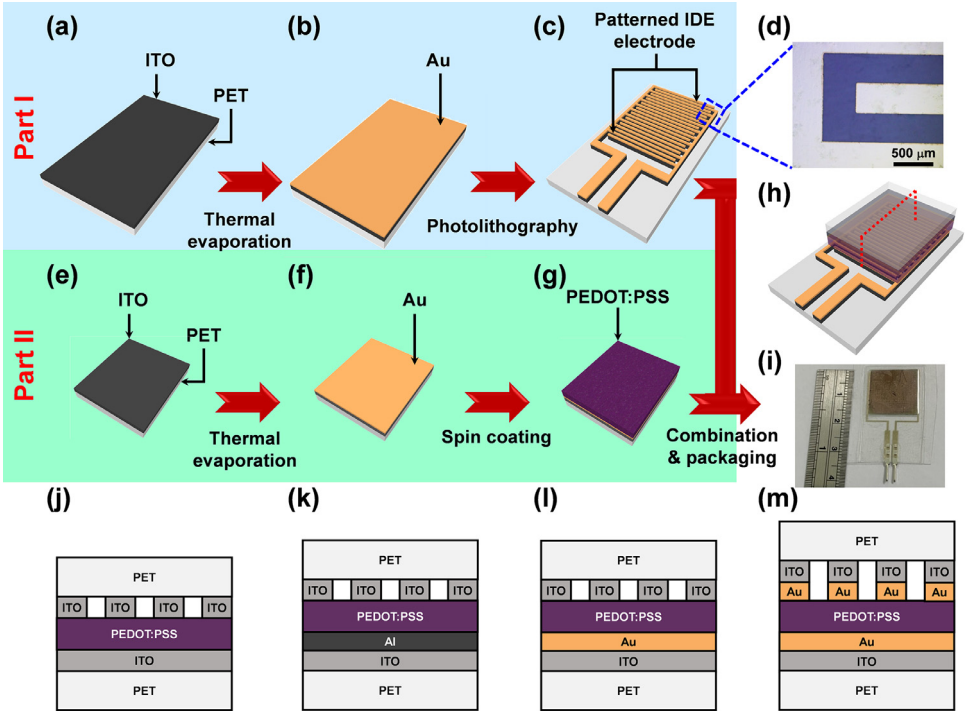

Fig. 1. Fabrication procedures of piezoresistive pressure sensing devices with an IDE structure by a combination of two parts, *i.e.*, parts I and II. (a)(e) ITO/PET substrate; (b)(f) Deposition of Al or Au films on ITO/PET substrates using a thermal coater; (c) Transferring of the pattern by a conventional photolithography method; (g) Performing of the PEDOT:PSS films on ITO/PET substrates with metallic interfacial layers at a spin speed of 500 rpm by spin-coating; (h) Combination of parts I and II to form the sandwich structure of pressure sensing device and packaged using a commercially available PET. The real-time photo image of the well-defined patterned electrode was shown in (d) using an optical microscope. The real-time image of the fabricated sensing device with a length of 1.6 cm was shown in (i). The cross-sectional diagrams of the piezoresistive pressure sensing devices (j) without and with (k) a single-sided Al interfacial layer, (l) single-sided Au interfacial layer, and (m) double-sided Au interfacial layer.

months, 3 months, and 6 months of fabrication were denoted as Days 1, 3, 7, 14, 21, 30, 60, 90, and 180, respectively. To investigate the changes in the film surface, the morphological and potential analyses of ITO/PET substrates, thermally coated Au and Al films, and spin-coated PEDOT:PSS films were performed via FE-SEM (SU8010, Hitachi High-Technologies Corp., Tokyo, Japan), atomic force microscopy (AFM) (Bruker AXS MultiMode 8, Bruker Corp., Billerica, USA), and Kelvin probe force microscopy (KPFM) (Dimension-3100 Multimode, Digital Instruments, Bresso, Italy). Additionally, the PEDOT:PSS films on the ITO/PET substrates with different metallic interfacial layers were examined via XPS analysis (ULVAC-PHI 5000 Versaprobe II system, ULVAC-PHI Inc., Kanagawa, Japan) and Raman spectroscopy (Micro Raman/PL/TR-PL spectrometer, ProTrustech Co., Ltd., Taiwan) to investigate the chemical reaction. Their effects on the piezoresistive behaviors were investigated by measuring the resistance change via applying a 0 – 20 kPa mechanical pressure on the sensing devices. The fabricated pressure-sensing devices were placed on a custom-developed sample holder made of rigid steel, and the pressure was applied using a vertical stand equipped with a force gage (JSV-H1000 Vertical Servo Stand, ALGOL Instrument Co., Ltd., Taiwan) through an Al tip. To apply a uniform pressure over the samples, a square quartz buffer of 1 cm^2 was inserted between the Al tip and the sensing devices. The pressure was applied at a rate of 2 mm/s to analyze the piezoresistive behavior, and the resistance was monitored using a Keithley 2450 interactive digital source meter (Keithley Instruments Inc., Solon, USA). Furthermore, the carrier conduction mechanism was realized via variable range hopping (VRH) measurements of the PEDOT:PSS films on ITO/PET substrates with different metallic interfacial layers. The low-temperature current-voltage characteristics were measured using a cryogenic probe station (CG-196CU, EverBeing International Corp., Taiwan). Finally, a theoretical model with carrier conduction pathways is proposed to interpret the material and electrical properties of packaged ITO/PEDOT:PSS/ITO piezoresistive pressure sensors with reaction-inhibited interfacial coatings.

3. Results and discussion

3.1. Surface morphological analysis of PEDOT:PSS films on ITO/PET substrates with reaction-inhibited interfacial coatings

Fig. 2 shows the topographical images of the ITO/PET substrates, thermally coated metallic interfacial layers, and spin-coated PEDOT:PSS films via FE-SEM at 100X magnification on Days 0 and 180. The pristine ITO film on the PET substrate exhibited an amorphous nature with micro-cracks, as shown in Fig. 2a, which was also reported by Lee et al. [45]. Meanwhile, for the samples with a thermally coated Al film on ITO/PET substrates, a compact and uniform film structure was obtained, as shown in Fig. 2b. As the thickness of the thermally coated Au film increased, the micro-cracks on the Au/ITO stacked films reduced significantly (Fig. 2c–e), contributing to a better reaction-inhibited behavior. After the spin-coating of PEDOT:PSS films on pristine ITO films and metallic interfacial layer-coated ITO films, a similar surface morphology was observed on Day 0 (Fig. 2f–j) in all samples. However, on Day 180, the PEDOT:PSS film on pristine ITO films presented multiple bright spots, whereas the films on the metallic interfacial layer-coated ITO films exhibited the same images as those on Day 0, as shown in Fig. 2k–o, because of the macroscopic phase separation and generation of highly resistive compounds caused by the reaction between PEDOT:PSS and ITO films [46,47]. To further confirm the surface morphology, AFM images of ITO/PET substrates, thermally coated metal interfacial layers, and spin-coated PEDOT:PSS films with a field of view of 5 μm × 5 μm on Days 0 and 180 were analyzed and are shown in Fig. S1. The surface roughness of the ITO films was measured to be 3.5 nm, whereas for the Al- and Au-coated ITO films, the surface roughness increased up to 5.39 nm (Fig.

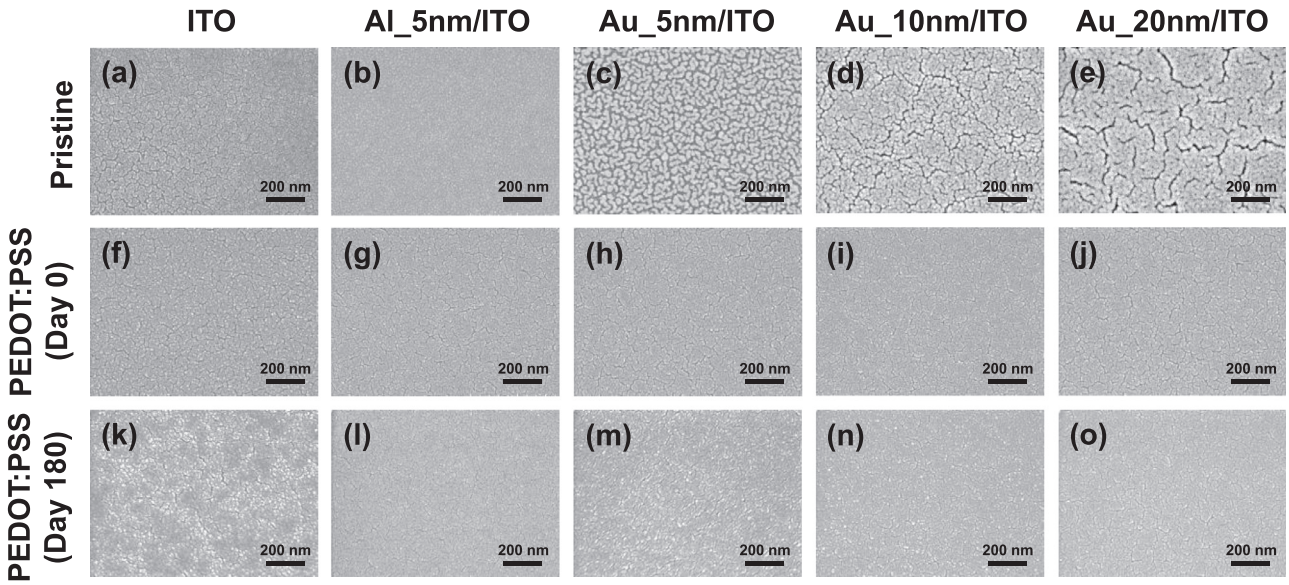

Fig. 2. FE-SEM images of (a) pristine ITO/PET substrate and with a metallic interfacial layer of (b) 5-nm-thick Al film, (c) 5-nm-thick Au film, (d) 10-nm-thick Au film, and (e) 20-nm-thick Au film, respectively. FE-SEM images of spin-coated PEDOT:PSS films on (f)(k) pristine ITO/PET substrate and with a metallic interfacial layer of (g)(l) 5-nm-thick Al film, (h)(m) 5-nm-thick Au film, (i)(n) 10-nm-thick Au film, and (j)(o) 20-nm-thick Au film, respectively, on Days 0 and 180.

S1a–e). Moreover, after spin-coating the PEDOT:PSS film, the surface roughness reduced to less than 1.99 nm, as shown in Fig. S1f–j, indicating the high uniformity of PEDOT:PSS films. However, on Day 180, the PEDOT:PSS films became rough in all the samples (Fig. S1k–o), owing to the high absorption coefficient of humidity of PEDOT:PSS films in a normal environment, as proposed by Muckley et al. [48]. This can be prevented by complete sealing via PET packaging, as shown in Fig. 1i.

3.2. Reliability behaviors of ITO/PEDOT:PSS/ITO piezoresistive pressure sensors with reaction-inhibited interfacial coatings

More than 20 samples were prepared for each case and stored in a normal environment for a particular time interval of measurement to investigate the time-dependent reliability of ITO/PEDOT:PSS/ITO piezoresistive pressure sensors with different metallic interfacial layers. Fig. 3a–c shows the R–P characteristics of the ITO/PEDOT:PSS/ITO pressure sensors without any metallic interfacial layer, with a single-sided 10-nm-thick Au interfacial layer, and with a double-sided 10-nm-thick Au interfacial layer, respectively, for a time interval of 6 months. A pressure of 0 – 20 kPa was applied to the samples to investigate the resistance change. The R–P curves of ITO/PEDOT:PSS/ITO pressure sensors with a single-sided 5-nm-thick Al interfacial layer, single-sided 5-nm-thick Au interfacial layer, and single-sided 20-nm-thick Au interfacial layer were measured and are presented in Fig. S2. The fabricated sensors exhibited an ideal piezoresistive pressure sensing behavior, *i.e.*, the resistance value decreased with the applied pressure for all samples. As the time interval of measurement increased, the resistance of the sample without any metallic interfacial layer increased significantly, as shown in Fig. 3a. At 20 kPa, the resistance increased by at least two orders of magnitude between Days 0 and 180, along with a distinct late piezoresistive response. Fortunately, a significant improvement in piezoresistive characteristics was observed in the samples with an Au interfacial layer between the PEDOT:PSS sensing membrane and ITO electrode, particularly in the sample with a double-sided 10-nm-thick Au interfacial layer (Fig. 3b,c and Fig. S2b,c). Between Days 0 and 180, stable piezoresistive characteristics with the reduction in resistance deviation were observed. Additionally, the piezoresistive pressure sensor with an Al interfacial layer showed a notable response delay, especially at long measurement times, as shown in Fig. S2a, which can be ascribed to the formation of a native Al_xO_y layer on the Al film surface in the environment [49]. Hence, the Al interfacial layer is not a suitable material for use in reaction-inhibited interfacial coatings of ITO/PEDOT:PSS/ITO piezoresistive pressure sensors and only the thickness of 5 nm was investigated in this study. Furthermore, the piezoresistive sensitivity of all samples at different time intervals of measurement can be calculated from the slopes of the R–P curves presented in Fig. 3a–c and Fig. S2a–c at pressures lower than 6 kPa using the following equation:

$$S = \frac{\log(R_0) - \log(R_{6kPa})}{6\ kPa} \quad (1)$$

where S is the piezoresistive sensitivity and R_0 and R_{6kPa} are the resistances when no pressure and a pressure of 6 kPa are applied, respectively. In the sample without any interfacial layer, the piezoresistive sensitivity decreased significantly as the time intervals of measurement increased, as shown in Fig. 3d. Furthermore, the pressure sensors with metallic interfacial layers exhibited moderate degradation in terms of piezoresistive sensitivity. To realize the change in piezoresistive sensitivity of the samples at each time interval, the sensitivity difference ratio, *i.e.*, $\Delta S/S_0$, was calculated as follows:

$$\frac{\Delta S}{S_0} = \frac{S_0 - S_d}{S_0} \quad (2)$$

where S_0 is the sensitivity of the pressure sensor on Day 0 and S_d is the sensitivity of the pressure sensor at a specific time interval of measurement. The sensitivity difference ratio as a function of the time intervals of measurement is plotted in Fig. 3e. Compared with the sample without any interfacial layer, the $\Delta S/S_0$ was much smaller for the ITO/PEDOT:PSS/ITO piezoresistive pressure sensors with metallic interfacial layers, indicating their high stability in terms of sensitivity. The variation in the resistance ($\Delta R/R_0$) between Days 0 and 180 of the PEDOT:PSS piezoresistive pressure sensors was calculated under pressures of 6 and 20 kPa respectively, and are shown in Fig. S3. A similar behavior was observed, *i.e.*, the samples with metallic interfacial layers can reduce the variation in resistance between Days 0 and 180. In addition, the coefficient of variation (CV), defined as the ratio of the sample standard deviation (s) to the sample mean ($\bar{x}$) of the resistance, is a standardized indication of dispersion of a probability distribution for expressing the stability and repeatability of ITO/PEDOT:PSS/ITO piezoresistive pressure sensors. To calculate

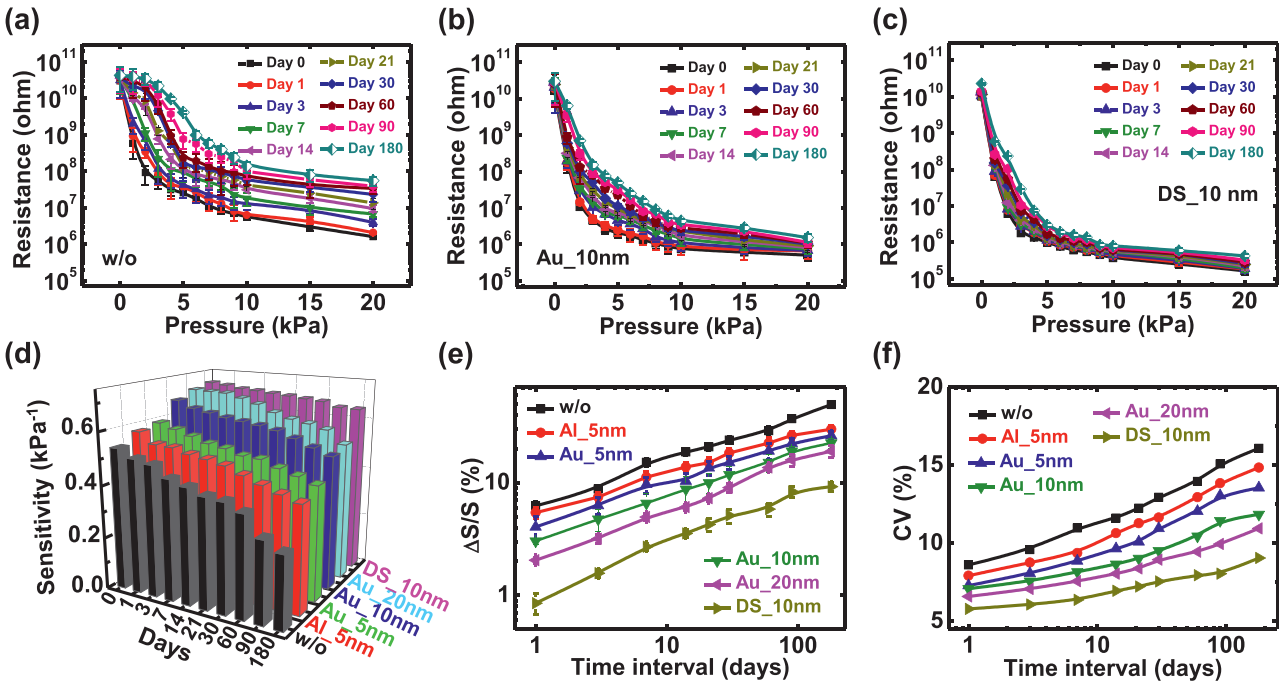

Fig. 3. *R–P* curves of the ITO/PEDOT:PSS/ITO piezoresistive pressure sensors (a) without and with (b) a single-sided 10-nm-thick Au interfacial layer and (c) double-sided 10-nm-thick Au interfacial layer for a time interval of 6 months. (d) 3D matrix in sensitivity of the ITO/PEDOT:PSS/ITO piezoresistive pressure sensors with different metallic interfacial layers and measurement time intervals. (e) Calculated sensitivity difference ratio ($\Delta S/S_0$) and (f) coefficient of variation (CV) as a function of measurement time interval of the ITO/PEDOT:PSS/ITO piezoresistive pressure sensors with different metallic interfacial layers.

the CV, more than 20 samples of each pressure sensor were measured for the entire time interval. In Fig. 3f, it was observed that the CV was low initially but increased significantly as the measurement time interval increased. The degradation can be ascribed to the large deviation in resistance and was particularly severe in the sample without any interfacial layer, where a CV exceeding 16% was recorded on Day 180. Meanwhile, for the sample with a double-sided 10-nm-thick Au interfacial layer, the CV can be improved significantly to less than 9% (on Day 180), which is adequate for future highly reliable piezoresistive pressure sensing applications.

Fig. 4a–c shows the reversible testing characteristics of loading/unloading cycles for the ITO/PEDOT:PSS/ITO piezoresistive pressure sensors without any metallic interfacial layer, with a single-sided 10-nm-thick Au interfacial layer, and with a double-sided 10-nm-thick Au interfacial layer, respectively. A fixed pressure of 20 kPa was applied for 400 cycles on Days 0 and 180. The reversible testing characteristics of ITO/PEDOT:PSS/ITO pressure sensors with a single-sided 5-nm-thick Al interfacial layer, single-sided 5-nm-thick Au interfacial layer, and single-sided 20-nm-thick Au interfacial layer were measured and are presented in Fig. S4a–c, respectively. To emphasize the differences, the first and last 50 cycles of the reversible testing characteristics were magnified, as shown in Fig. 4d–f and Fig. S4d–f. On Day 0, all devices demonstrated stable switching throughout the loading/unloading cycles. Meanwhile, the resistance on Day 180 increased by least one order of magnitude at the end of 400 cycles for the ITO/PEDOT:PSS/ITO pressure sensor without any metallic interfacial layer. The instability in resistance under loading/unloading cycles can be improved notably by depositing a metallic interfacial layer between the PEDOT:PSS sensing membrane and ITO electrode, particularly in the sample with a double-sided 10-nm-thick Au interfacial layer, as shown in Fig. 4c,f. The data presented above indicate that conventional ITO/PEDOT:PSS/ITO piezoresistive pressure sensors suffer from a severe time-dependent reliability degradation, resulting in a high possibility of device failure after prolonged usage; however, this can be effectively solved by applying a cost-effective Au interfacial coating of 10 – 20 nm. For the reliability testing of the ITO/PEDOT:PSS/ITO piezoresistive pressure sensors at high temperature or under high humidity conditions, the reaction-inhibition behaviors of the metallic interfacial coating might get worse, which could be investigated in future.

3.3. Time-dependent material analysis of PEDOT:PSS films on ITO/PET substrates with reaction-inhibited interfacial coatings

To determine the factors contributing to the time-dependent reliability degradation, changes in the material properties of the PEDOT:PSS sensing membrane and ITO electrode were analyzed via XPS and Raman spectroscopy at different time intervals of measurement. Fig. 5a and Fig. S5 show the O 1*s* XPS spectra of the PEDOT:PSS films on ITO/PET substrates with and without metallic interfacial layers on Days 0, 90, and 180. A faster spin-coating of 3000 rpm was performed for 15 s to obtain a thinner PEDOT:PSS film (90 nm), and the film was sputtered using Ar plasma for 2 min to investigate the material changes in the PEDOT:PSS films at a depth of 80 nm from the film surface. The primary deconvoluted peaks in the O 1*s* spectra were obtained at 531.8, 532, and 533 eV, corresponding to S=O, O–H, and C–O–C bonds, respectively [50–52]. As shown in Fig. 5a, when the time interval of measurement increased, the intensity of the O–H peak increased significantly, which can be attributed to the ease of water absorption of PEDOT:PSS in air [49]. The hygroscopicity of PEDOT:PSS films can be prevented via complete sealing using PET, as shown in Fig. 1i. An additional peak at 531.2 eV was observed for the PEDOT:PSS film on the ITO electrode, and it belonged to the In–O–H bond caused by the doping of In into PEDOT:PSS from the ITO electrode [53]. Compared with Day 90, the intensity of the In–O–H peak increased on Day 180, indicating that In doping into PEDOT:PSS would be more significant as the time intervals increase. Moreover, no In–O–H peak appeared for the PEDOT:PSS films on the ITO electrode with metallic interfacial layers. However, as shown in Fig. S5, the PEDOT:PSS film on the ITO electrode with a 5-nm-thick Al interfacial layer presented an Al–O–Al bond at 531 eV, which belonged to the native Al_xO_y layer on the Al film surface [54]. The presence of the

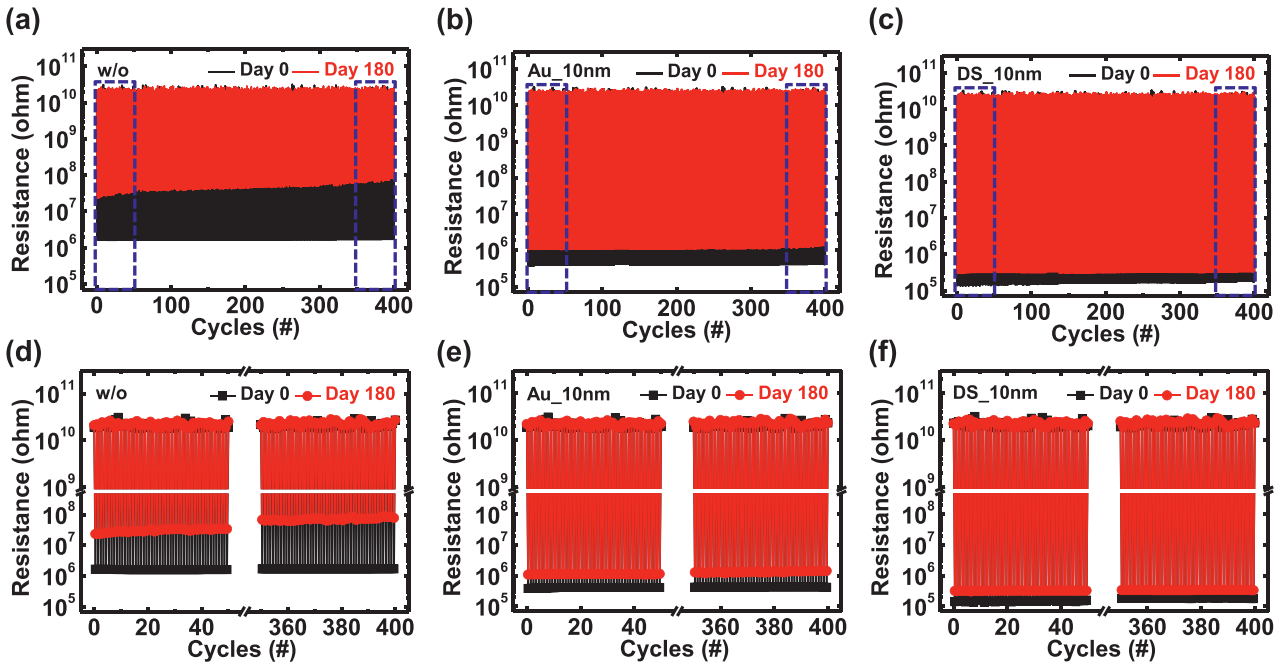

Fig. 4. Reversible testing characteristics of loading/unloading cycles for the ITO/PEDOT:PSS/ITO piezoresistive pressure sensors (a) without and with (b) a single-sided 10-nm-thick Au interfacial layer and (c) double-sided 10-nm-thick Au interfacial layer on Days 0 and 180. The first and last 50 cycles of the reversible testing characteristics for the ITO/PEDOT:PSS/ITO piezoresistive pressure sensors (d) without and with (e) a single-sided 10-nm-thick Au interfacial layer and (f) double-sided 10-nm-thick Au interfacial layer on Days 0 and 180.

Al_xO_y layer might be responsible for the response delay of the piezoresistive pressure sensors with a 5-nm-thick Al interfacial layer, as shown in Fig. S2a. Additionally, the In 3*d* XPS spectra of the PEDOT:PSS films on ITO/PET substrates were compared, as shown in Fig. 5b. Two components of binding energy at approximately 445.5 and 453.1 eV, belonging to In $3d_{5/2}$ and In $3d_{3/2}$ of the oxidation state of indium (In–O), respectively, were observed [55]. On Day 0, the intensity of the In 3*d* spectra of the PEDOT:PSS films on ITO/PET substrates without any metallic interfacial layer was higher than those of the other samples. For the samples with metallic interfacial layers, the intensity of the In–O bond at the PEDOT:PSS and ITO interface can be reduced effectively, particularly in the sample with a 5-nm-thick Al interfacial layer. This reduction is attributable to the presence of a native and dense Al_xO_y layer on the Al film surface for preventing In–O diffusion. As the time interval of measurement increased, the intensity of the In–O bond increased, particularly in the sample without any metallic interfacial layer, thereby resulting in time-dependent reliability issues in the ITO/PEDOT:PSS/ITO piezoresistive pressure sensors, as discussed in the previous section.

Fig. 5c,d and Fig. S6 present the Raman spectra of the PEDOT:PSS films on ITO/PET substrates with and without metallic interfacial layers on Days 0, 90, and 180. For the PEDOT:PSS film without any metallic interfacial layer (Fig. 5c), the primary bands were symmetric C_α=C_β stretching vibrations at 1440 cm^{-1}; asymmetric C_α=C_β stretching vibrations from the thiophene rings in the middle and end of the PEDOT chains at 1498 and 1591 cm^{-1}, respectively; C_α–C_α inter-ring vibrations at 1256 cm^{-1}; and C_β–C_β stretching vibrations at 1365 cm^{-1} [56–59]. When the time interval of measurement increased, the main peaks shifted toward lower wave numbers, owing to the longer bond length [60]. Both the PEDOT oligomers and PSS chains were modified by In ions from indium hydroxide (In–O–H), thereby modifying the bond length of the PEDOT:PSS chains. Fortunately, the Raman peaks of the samples with metallic interfacial layers did not shift, as shown in Fig. 5d and Fig. S6, thereby proving that the bond length of the PEDOT:PSS chains remained unchanged because of the effective suppression of In diffusion via metallic interfacial layers.

The VRH distances of the PEDOT:PSS films on ITO/PET substrates with and without metallic interfacial layers on Days 0 and 180 were measured and are plotted in Fig. 5e. The temperature-dependent conductance, $G(T)$, of the PEDOT:PSS films were used to determine the VRH distance and can be described by Mott's law, as follows [61]:

$$G(T) = G_0\left[-\left(\frac{T_0}{T}\right)^{\gamma}\right] \quad (3)$$

where G_0 is the conductance pre-factor, T_0 is the characteristic temperature, T is the measurement temperature (230 – 300 K), and γ is an exponent related to the carrier transport process in PEDOT:PSS films on ITO/PET substrates with and without metallic interfacial layers. For VRH analysis, the exponent γ is expressed as $1/(d+1)$, where d is the dimensionality for the carrier conduction [62]. For the PEDOT:PSS films, a three-dimensional VRH is suggested, indicating $\gamma = 1/4$. Hence, the conductance *vs.* $T^{-1/4}$ characteristics were linearly fitted and the T_0 can be extracted from the slopes of the curves, as shown in the inset of Fig. 5e. The relationship between T_0 and the density of states at the Fermi level, $g(E_F)$, was established using Eq. (4):

$$T_0 = \frac{\beta}{g(E_F)\xi^3 k_B} \quad (4)$$

where ξ is the localization length, β is a numerical factor with the value of 21.2, and k_B is the Boltzmann constant [61]. Subsequently, $g(E_F)$ can be extracted based on T_0, and the hopping distance (l_0) can be calculated using Eq. (5) [63]:

$$l_0 = \left\{\frac{3}{2\alpha\left(\frac{4\pi}{3}\right)g(E_F)k_BT}\right\}^{1/4} \quad (5)$$

where α, which is equal to $1/\xi$, is the decay rate of the wave function [64]. The PEDOT:PSS films on ITO/PET substrates without and with metallic interfacial layers showed an average hopping distance value of 15.53 to 14.34 nm on Day 0, which is similar to that proposed by Nardes et al. [65]. On Day 180, the hopping distance of the PEDOT:PSS films on ITO/PET substrates without metallic interfacial layer

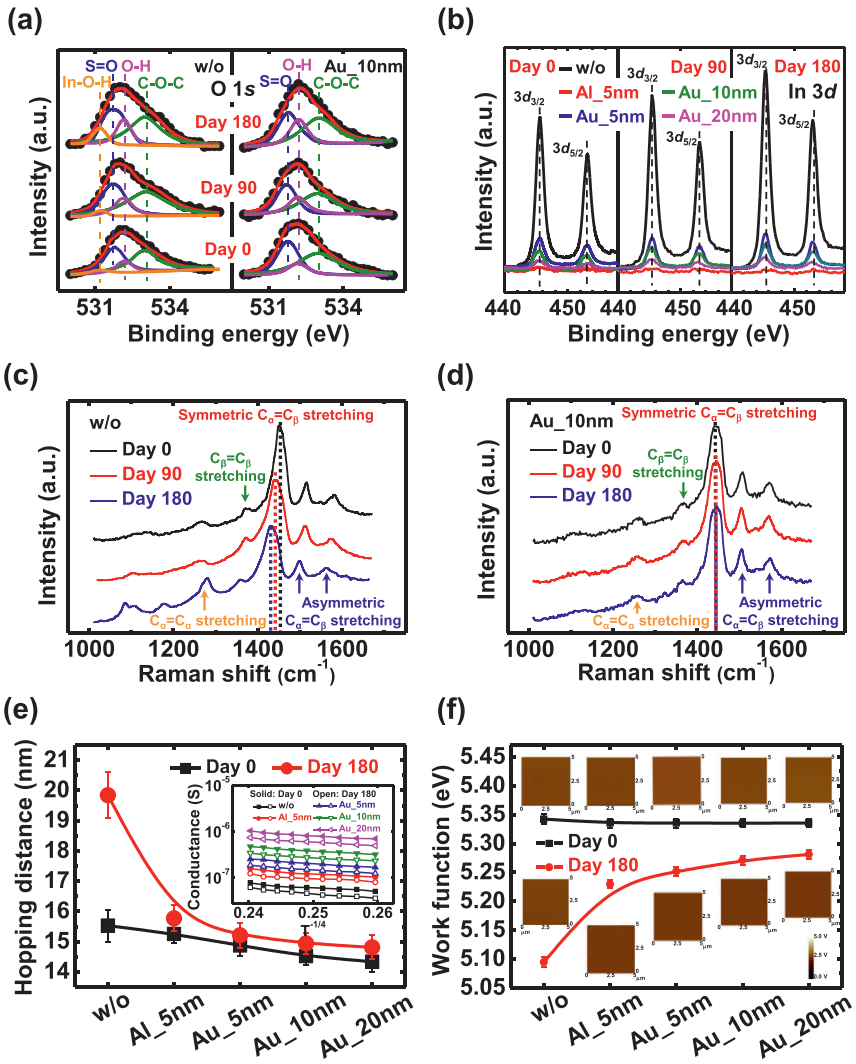

Fig. 5. (a) O 1 *s* XPS spectra of the PEDOT:PSS films at a depth of 10 nm from the ITO interface with and without a 10-nm-thick Au interfacial layer on Days 0, 90, and 180. (b) In 3*d* XPS spectra of the PEDOT:PSS films at a depth of 10 nm from the ITO interface with and without metallic interfacial layers on Days 0, 90, and 180. Raman spectra of the PEDOT:PSS films on ITO/PET substrates (c) without and (d) with a 10-nm-thick Au interfacial layer on Days 0, 90, and 180. (e) VRH distance of the PEDOT:PSS films on ITO/PET substrates with and without metallic interfacial layers on Days 0 and 180. The inset shows the linear fitting of G–$T^{-1/4}$ curves for all samples on Days 0 and 180. (f) Work function of the PEDOT:PSS films on ITO/PET substrates with and without metallic interfacial layers on Days 0 and 180. The inset shows the CPD images of all samples on Days 0 and 180.

increased significantly to 19.84 nm, whereas those of the films with metallic interfacial layers showed a relatively low deviation in terms of the hopping distance, as observed in Fig. 5e. This increment in hopping distance is a clear indication that the properties of PEDOT:PSS copolymers are influenced by the formation of highly resistive indium salts because In_2O_3 in ITO can be dissolved in acidic solutions such as PEDOT:PSS [47,66,67], as revealed in Fig. 5a, leading to the time-dependent reaction of PEDOT:PSS films on the ITO layer.

To further identify the effect of the ITO layer on PEDOT:PSS copolymers, KPFM measurements were performed, and the contact potential difference (CPD) between the reference Pt/Ir tip and the surface potential of the PEDOT:PSS films was obtained using the following formula:

$$\mathrm{CPD} = \frac{(\phi_{\mathrm{tip}} - \phi_{\mathrm{s}})}{\mathrm{e}} \tag{6}$$

where ϕ_{tip} and ϕ_{s} are the work functions of the reference tip and PEDOT:PSS films, respectively, and e is the charge of an electron. Before the measurement, a gold reference sample was used to calibrate the work function of the Pt/Ir coated tip for approximately 5.1 eV [68]. The CPD images and calculated work function of the PEDOT:PSS films on ITO/PET substrates with and without metallic interfacial layers on Days 0 and 180 are presented in Fig. 5f. At least 20 samples of each stacked film were investigated for statistical analysis. On Day 0, an average work function of 5.34 eV was obtained, *i.e.*, within the range of 4.7 to 5.4 eV for pristine PEDOT:PSS films [69]. However, on Day 180, a lower work function was observed, particularly in the PEDOT:PSS film on the ITO/PET substrate without any metallic interfacial layer (5.09 eV). The extremely low work function on Day 180 can be ascribed to the reaction of PEDOT:PSS films on ITO layers, *i.e.*, the dissolution of In_2O_3 from ITO in acid PEDOT:PSS, where the work function of In_2O_3 is approximately 5.0 eV [70]. For the samples with metallic interfacial layers, the average work function values on Day 180 were 5.23 to 5.27 eV, which were slightly lower than that of pristine sample, because of the absorption of humidity in the PEDOT:PSS films when they were exposed to a normal environment [49,71].

3.4. Carrier transportation mechanisms of ITO/PEDOT:PSS/ITO piezoresistive pressure sensors with reaction-inhibited interfacial coatings

Fig. 6a illustrates the schematic of surface and interface reaction mechanisms of the PEDOT:PSS film on the ITO layer in a normal

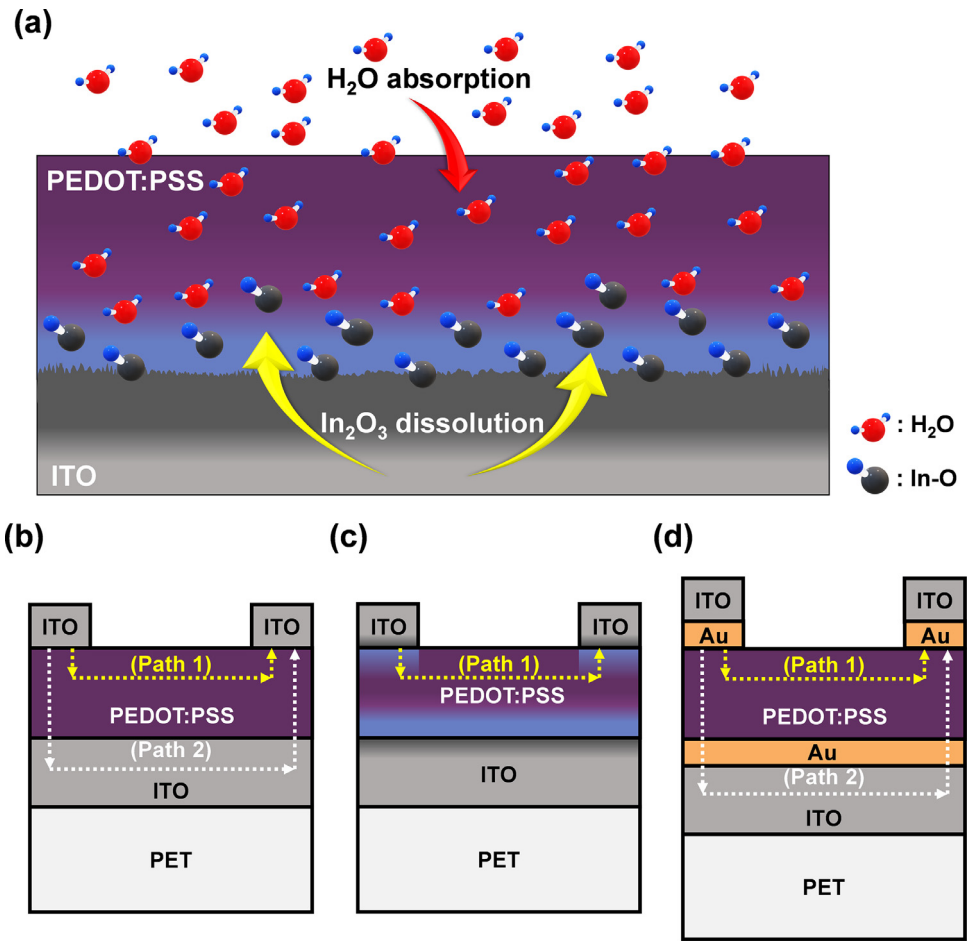

Fig. 6. (a) Schematic diagram of the surface and interface reaction mechanisms of the PEDOT:PSS film on the ITO layer in a normal environment. Schematic diagrams of the carrier conducting pathways of the ITO/PEDOT:PSS/ITO piezoresistive pressure sensors without metallic interfacial layer on Days (b) 0 and (c) 180, and (d) with a double-sided 10-nm-thick Au interfacial layer on Day 180.

environment. When the time interval of measurement increased, the dissolution of In_2O_3 from the ITO layer in the acidic PEDOT:PSS film became more active, thereby contributing to the degradation of sensitivity and stability in the ITO/PEDOT:PSS/ITO piezoresistive pressure sensors. Furthermore, as discussed previously, the absorption of humidity in PEDOT:PSS films occurs easily in a normal environment and worsen the reliability of the pressure sensors. Hence, a complete sealing of the devices via PET packaging, as displayed in Fig. 1i, is inevitable. For conventional piezoresistive pressure sensors with an IDE electrode structure, two conductive pathways have been proposed to achieve superior electrical behaviors [72], as shown in Fig. 6b. However, after a long time interval of measurement, interface reaction occurred between the PEDOT:PSS sensing membrane and ITO electrode, and some highly resistive indium salts formed and diffused into the PEDOT:PSS films. The increase in resistance of the PEDOT:PSS copolymers at the ITO interface interrupted the second conductive pathway (Fig. 6c), resulting in deteriorated piezoresistive pressure sensing characteristics, as shown in Figs. 3 and 4. Hence, a reaction-inhibited Au interfacial coating between the PEDOT:PSS sensing membrane and ITO electrode is proposed, as presented in Fig. 6d, which is promising for future highly reliable piezoresistive pressure sensors. The comparison on the device structures, issues and solutions of the time-dependent instability, temperature or environment, and measurement time intervals of piezoresistive pressure sensors between this study and some published works was made and is shown in Table S1 to emphasize the robustness of Au interfacial coating and PET packaging on the reliability of ITO/PEDOT:PSS/ITO piezoresistive pressure sensors.

4. Conclusion

In summary, reaction-inhibited interfacial coatings were successfully implemented in ITO/PEDOT:PSS/ITO piezoresistive pressure sensors to demonstrate robust sensitivity and reliability characteristics over a long time interval of measurement. To maintain desirable piezoresistive properties, various metallic materials and thicknesses were optimized at the interface between the PEDOT:PSS sensing membrane and ITO electrode. Subsequently, the PEDOT:PSS films on ITO layers with different metallic interfacial coatings were analyzed via material analysis methods, such as XPS, FE-SEM, AFM, Raman spectroscopy, and KPFM. After using metallic interfacial coatings, the bright spots in the SEM images and In–O–H bonds in the XPS spectra of the PEDOT:PSS films were reduced significantly, indicating the suppression of the dissolution of In_2O_3 from ITO layers in acidic PEDOT:PSS copolymers. In addition, a complete sealing of the piezoresistive pressure sensors using PET packaging was conducted to effectively reduce the absorption of humidity in the PEDOT:PSS films even after a measurement time interval of 6 months; this is useful for demonstrating the robust piezoresistive pressure sensing behaviors. Among the samples, those devices with a 10-nm-thick double-sided Au interfacial layer exhibited a low sensitivity deviation of 9.22% and stable cycling tests for more than 400 times, indicating that the

reaction-inhibited interfacial coatings between PEDOT:PSS and ITO can be applied in future flexible pressure sensing technologies.

Declaration of Competing Interest

The authors declare that they have no known competing financial interests or personal relationships that could have appeared to influence the work reported in this paper.

Acknowledgments

This research was supported by Ministry of Science and Technology, R.O.C. (Contract No. of MOST 109–2221-E-182–032) and Chang Gung Memorial Hospital, Linkou, Taiwan (Contract Nos. of CMRPD2H0133, CMRPD2J0052, and BMRPA74).

Credit authorship contribution statement

Jer-Chyi Wang: Conceptualization, Methodology, Writing - Review & Editing, Supervision. Rajat Subhra Karmakar: Investigation, Validation, Data Curation, Writing- Original Draft Preparation. Ting-Han Lin: Investigation. Ming-Chung Wu: Methodology, Resources. Kuo-Hsuan Chang: Conceptualization, Supervision.

Supplementary materials

Supplementary material associated with this article can be found in the online version at doi:10.1016/j.jtice.2021.07.004.

References

[1] Dubal DP. Advances in flexible supercapacitors for portable and wearable smart gadgets. Amsterdam: Elsevier; 2018. p. 209–46.
[2] Zou M, Ma Y, Yuan X, Hu Y, Liu J, Ji Z. Flexible devices: from materials, architectures to applications. J Semicond 2018;39:011010.
[3] Cho EC, Chang-Jian CW, Huang JH, Wu RT, Lu CZ, Lee KC, et al. Laser scribing of Ag-decorated graphene for high-performance and flexible heaters. J Taiwan Inst Chem Eng 2021;119:224–31.
[4] Yan K, Li J, Pan L, Shi Y. Inkjet printing for flexible and wearable electronics. APL Mater 2020;8:120705.
[5] Maddipatla D, Narakathu BB, Atashbar M. Recent progress in manufacturing techniques of printed and flexible sensors: a review. Biosensors 2020;10:199.
[6] Li L, Zheng J, Chen J, Luo Z, Su Y, Tang W, et al. Flexible pressure sensors for biomedical applications: from ex vivo to in vivo. Adv Mater Interfaces 2020;7:2000743.
[7] Cheng MY, Lin CL, Lai YT, Yang YJ. A polymer-based capacitive sensing array for normal and shear force measurement. Sensors 2010;10:10211–25.
[8] Hsiao FR, Wu IF, Liao YC. Porous CNT/rubber composite for resistive pressure sensor. J Taiwan Inst Chem Eng 2019;102:387–93.
[9] Ngo HD, Mackowiack P, Grabbert N, Weiland T, Hu X, Schneider-Ramelow M, Ehrmann O, Lang KD. The roadmap for development of piezoresistive micro mechanical sensors for harsh environment applications. 11th International Conference on Sensing Technology; 2017. p. 1–6.
[10] Mishra RB, El-Atab N, Hussain AM, Hussain MM. Recent progress on flexible capacitive pressure sensors: from design and materials to applications. Adv Mater Technol 2021;6:2170023.
[11] Wang S, Li Q, Feng S, Lv Y, Zhang T. A water-retaining, self-healing hydrogel as ionic skin with a highly pressure sensitive properties. J Taiwan Inst Chem Eng 2019;104:318–29.
[12] Wang JC, Jiang YP, Lin CH, Chan SH, Wu MC. Enhanced piezoelectric tactile sensing behaviors of high-density and low-damage CF_4-plasma-treated IGZO thin-film transistors coated by P(VDF-TrFE) copolymers. Sens Actuator A-Phys 2020;304:111855.
[13] Wang JC, Karmakar RS, Lu YJ, Chan SH, Wu MC, Lin KJ, et al. Miniaturized flexible piezoresistive pressure sensors: poly(3,4-ethylenedioxythiophene):poly(styrenesulfonate) copolymers blended with graphene oxide for biomedical applications. ACS Appl Mater Interfaces 2019;11:34305–15.
[14] Trifigny N, Kelly F, Cochrane C, Boussu F, Koncar V, Soulat D. PEDOT:PSS-based piezoresistive sensors applied to reinforcement glass fibres for in situ measurement during the composite material weaving process. Sensors 2013;13:10749–64.
[15] Cruz S, Rocha LA, Viana JC. Piezo-resistive behaviour at high strain levels of PEDOT:PSS printed on a flexible polymeric substrate by a novel surface treatment. J Mater Sci: Mater Electron 2017;28:2563–73.
[16] Ding Y, Yang J, Tolle CR, Zhu Z. Flexible and compressible PEDOT:PSS@Melamine conductive sponge prepared via one-step dip coating as piezoresistive pressure sensor for human motion detection. ACS Appl Mater Interfaces 2018;10:16077–86.
[17] Skotheim T, Reynolds J. Handbook of conducting polymers. 3rd ed. NY: CRC Press; 2007.
[18] Elschner A, Kirchmeyer S, Lovenich W, Merker U, Reuter K. PEDOT: principles and applications of an intrinsically conductive polymer. NY: CRC Press; 2010.
[19] Hegde R, Ramji K, Peravali S, Shiralgi Y, Hegde G, Bathini L. Characterization of MWCNT-PEDOT:PSS nanocomposite flexible thin film for piezoresistive strain sensing application. Adv Polym Technol 2019;2019:9320976.
[20] Hegde R, Ramji K, Peravali S, Hegde G. Synthesis of carbon nanospheres and piezoresistive study of carbon nanospheres-PEDOT:PSS nanocomposite flexible thin film for strain sensing applications. Mater Res Express 2019;6:076408.
[21] Sofi AH, Shah MA, Asokan K. Structural, optical and electrical properties of ITO thin films. J Electron Mater 2018;47:1344–52.
[22] Eshaghi A, Graeli A. Optical and electrical properties of indium tin oxide (ITO) nanostructured thin films deposited on polycarbonate substrates "thickness effect". Optik (Stuttg) 2014;125:1478–81.
[23] Yang HJ, Chen CH, Wu KY, Fan CM, Wu CL, Huang CF, et al. Improvement of optical and electrical properties of Boron-doped ZnO films by ITO buffer layers for photovoltaic application. J Taiwan Inst Chem Eng 2014;45:3016–20.
[24] Anithaa AC, Asokan K, Sekar C. Low energy nitrogen ion beam implanted tungsten trioxide thin films modified indium tin oxide electrode based acetylcholine sensor. J Taiwan Inst Chem Eng 2018;84:11–8.
[25] Chen Z, Li W, Li R, Zhang Y, Xu G, Cheng H. Fabrication of highly transparent and conductive indium–tin oxide thin films with a high figure of merit via solution processing. Langmuir 2013;29:13836–42.
[26] Kim SM, Kim CH, Kim Y, Kim N, Lee WJ, Lee EH, et al. Influence of PEDOT:PSS crystallinity and composition on electrochemical transistor performance and long-term stability. Nat Commun 2018;9:3858.
[27] Fan X, Nie W, Tsai H, Wang N, Huang H, Cheng Y, et al. PEDOT:PSS for flexible and stretchable electronics: modifications, strategies, and applications. Adv Sci 2019;6:1900813.
[28] Yin HE, Huang FH, Chiu WY. Hydrophobic and flexible conductive films consisting of PEDOT:PSS-PBA/fluorine-modified silica and their performance in weather stability. J Mater Chem 2012;22:14042–51.
[29] Lin CH, Sun KW, Liu QM, Shirai H, Lee CP. Poly(3,4-ethylenedioxythiophene):poly (styrenesulfonate)/GaAs hybrid solar cells with 13% power conversion efficiency using front- and back-surface field. Opt Express 2015;23:A1051–9.
[30] Nardes AM, Kemerink M, Janssen RAJ, Bastiaansen JAM, Kiggen NMM, Langeveld BMW, et al. Microscopic understanding of the anisotropic conductivity of PEDOT:PSS thin films. Adv Mater 2007;19:1196–200.
[31] Huang J, Miller PF, Wilson JS, de Mello AJ, de Mello JC, Bradley DDC. Investigation of the effects of doping and post-deposition treatments on the conductivity, morphology, and work function of poly(3,4-ethylenedioxythiophene)/poly(styrene sulfonate) films. Adv Funct Mater 2005;15:290–6.
[32] Chacko AP, Jin Y, Shi Y, Bunha A, Chen J, Lessner P. Advances in reliability of conducting polymers and conducting polymer based capacitors in high humidity environment. ECS Trans 2018;85:115–27.
[33] Hou X, Li Q, Cheng T, Yu L, Wang F, Lin J, et al. Improvement of the power conversion efficiency and long term stability of polymer solar cells by incorporation of amphiphilic Nafion doped PEDOT:PSS as a hole extraction layer. J Mater Chem A 2015;3:18727–34.
[34] Zhu Z, Yang G, Li R, Pan T. Photopatternable PEDOT:PSS/PEG hybrid thin film with moisture stability and sensitivity. Microsyst Nanoeng 2017;3:17004.
[35] Hakansson A, Han S, Wang S, Lu J, Braun S, Fahlman M, et al. Effect of (3-Glycidyloxypropyl)Trimethoxysilane (GOPS) on the electrical properties of PEDOT:PSS films. J Polym Sci Pt B-Polym Phys 2017;55:814–20.
[36] Solazzo M, Krukiewicz K, Zhussupbekova A, Fleischer K, Biggscg MJ, Monaghan MG. PEDOT:PSS interfaces stabilised using a PEGylated crosslinker yield improved conductivity and biocompatibility. J Mater Chem B 2019;7:4811–20.
[37] Liu X, Zai J, Iqbal A, Chen M, Ali N, Qi R, et al. Glycerol-crosslinked PEDOT:PSS as bifunctional binder for Si anodes: improved interfacial compatibility and conductivity. J Colloid Interface Sci 2020;565:270–7.
[38] Zhang S, Kumar P, Nouas AS, Fontaine L, Tang H, Cicoira F. Solvent-induced changes in PEDOT:PSS films for organic electrochemical transistors. APL Mater 2015;3:014911.
[39] Yang W, Broski A, Wu J, Fan QH, Li W. Characteristics of transparent, PEDOT:PSS-coated indium-tin-oxide (ITO) microelectrodes. IEEE Trans Nanotechnol 2018;17:701–4.
[40] Cameron J, Skabara PJ. The damaging effects of the acidity in PEDOT:PSS on semiconductor device performance and solutions based on non-acidic alternatives. Mater Horiz 2020;7:1759–72.
[41] Wong KW, Yip HL, Luo Y, Wong KY, Lau WM, Low KH, et al. Blocking reactions between indium tin oxide and poly (3,4-ethylene dioxythiophene):poly (styrene sulphonate) with a self-assembly monolayer. Appl Phys Lett 2002;80:2788–91.
[42] Liu T, Jiang F, Qin F, Meng W, Jiang Y, Xiong S, et al. Nonreduction-active hole-transporting layers enhancing open-circuit voltage and efficiency of planar perovskite solar cells. ACS Appl Mater Interfaces 2016;8:33899–906.
[43] Xu J, Wang Y, Chen Q, Lin Y, Shan H, Roy VAL, et al. Enhanced lifetime of organic light-emitting diodes using soluble tetraalkyl-substituted copper phthalocyanines as anode buffer layers. J Mater Chem C 2016;4:7377–82.
[44] Ke L, Kumar RS, Chen P, Shen L, Chua SJ, Burden AP. Au-ITO anode for efficient polymer light-emitting device operation. IEEE Photonics Technol Lett 2005;17:543–5.
[45] Lee JR, Lee DY, Kim DG, Lee GH, Kim YD, Song PK. Characteristics of ITO films deposited on a PET substrate under various deposition conditions. Met Mater-Int 2008;14:745–51.

[46] Noh JS. Highly conductive and stretchable poly(dimethylsiloxane):poly(3,4-ethylenedioxythiophene):poly(styrene sulfonic acid) blends for organic interconnects. RSC Adv 2014;4:1857–63.
[47] Jo SJ, Kim CS, Kim JB, Ryu SY, Noh JH, Baik HK, et al. Increase in indium diffusion by tetrafluoromethane plasma treatment and its effects on the device performance of polymer light-emitting diodes. J Appl Phys 2008;103:114502.
[48] Muckley ES, Jacobs CB, Vidal K, Mahalik JP, Kumar R, Sumpter BG, et al. New insights on electro-optical response of poly(3,4-ethylenedioxythiophene):poly (styrenesulfonate) film to humidity. ACS Appl Mater Interfaces 2017;9:15880–6.
[49] Tiwari B, Bean JA, Szakmány G, Bernstein GH, Fay P, Porod W. Controlled etching and regrowth of tunnel oxide for antenna-coupled metal-oxide-metal diodes. J Vac Sci Technol B 2009;27:2153–60.
[50] Briggs D, Beamson G. XPS studies of the oxygen 1s and 2s levels in a wide range of functional polymers. Anal Chem 1993;65:1517–23.
[51] Petraki F, Kennou S, Nespurek S, Biler M. A spectroscopic study for the application of a PEDOT-type material as buffer layer in electronic devices. Org Electron 2010;11:1423–31.
[52] Moulder JF, Stickle WF, Sobol PE, Bomben KD. Handbook of X-ray photoelectron spectroscopy. Eden Prairie, MN: Perkin-Elmer Corp.; 1992.
[53] Park SY, Heo J, Yoon YJ, Kim JW, Jang H, Walker B, et al. Synergistic combination of amorphous indium oxide with tantalum pentoxide for efficient electron transport in low-power electronics. J Mater Chem C 2019;7:4559–66.
[54] Yang CS, Kim JS, Choi JW, Kwon MH, Kim YJ, Choi JG, et al. XPS study of aluminum oxides deposited on PET thin films. J Ind Eng Chem 2000;6:149–56.
[55] Khan GG, Ghosh S, Sarkar A, Mandal G, Mukherjee GD, Manju U, et al. Defect engineered d° ferromagnetism in tin-doped indium oxide nanostructures and nanocrystalline thin-films. J Appl Phys 2015;118:074303.
[56] Xu B, Gopalan SA, Gopalan AI, Muthuchamy N, Lee KP, Lee JS, et al. Functional solid additive modified PEDOT:PSS as an anode buffer layer for enhanced photovoltaic performance and stability in polymer solar cells. Sci Rep 2017;7:45079.
[57] Goutham Raj P, Sandhya Rani V, Kanwat A, Jang J. Enhanced organic photovoltaic properties via structural modifications in PEDOT:PSS due to graphene oxide doping. Mater Res Bull 2016;74:346–52.
[58] Lindfors T, Boeva ZA, Latonen RM. Electrochemical synthesis of poly(3,4-ethylenedioxythiophene) in aqueous dispersion of high porosity reduced graphene oxide. RSC Adv 2014;4:25279–86.
[59] Singh V, Arora S, Arora M, Sharma V, Tandon RP. Characterization of doped PEDOT:PSS and its influence on the performance and degradation of organic solar cells. Semicond Sci Technol 2014;29:045020.
[60] Popović L, de Waal D, Boeyens JCA. Correlation between Raman wavenumbers and P–O bond lengths in crystalline inorganic phosphates. J Raman Spectrosc 2005;36:2–11.
[61] Fogler MM, Teber S, Shklovskii BI. Variable-range hopping in quasi-one-dimensional electron crystals. Phys Rev B 2004;69:035413.
[62] Vitoratos E, Sakkopoulos S, Dalas E, Paliatsas N, Karageorgopoulos D, Petraki F, et al. Thermal degradation mechanisms of PEDOT:PSS. Org Electron 2009;10:61–6.
[63] Bai Y, Wu H, Wu R, Zhang Y, Deng N, Yu Z, et al. Study of multi-level characteristics for 3D vertical resistive switching memory. Sci Rep 2014;4:5780.
[64] Entin-Wohlman O, Gefen Y, Shapira Y. Variable-range hopping conductivity in granular materials. J Phys C 1983;16:1161.
[65] Nardes AM, Kemerink M, Janssen RAJ. Anisotropic hopping conduction in spin-coated PEDOT:PSS thin films. Phys Rev B 2007;76:085208.
[66] Chang CH, Chen SA. Effect of ionization potential change in poly(3,4-ethylenedioxythiophene):poly(styrenesulfonic acid) on the performance of polymer light emitting diodes due to its reaction with indium tin oxide. Appl Phys Lett 2007;91:103514.
[67] Nguyen TP, de Vos SA. An investigation into the effect of chemical and thermal treatments on the structural changes of poly(3,4-ethylenedioxythiophene)/polystyrenesulfonate and consequences on its use on indium tin oxide substrates. Appl Surf Sci 2004;221:330–9.
[68] Eastman DE. Photoelectric work functions of transition, rare-earth, and noble metals. Phys Rev B 1970;2:1–2.
[69] Sapp S, Luebben S, Losovyj YaB, Jeppson P, Schulz DL, Caruso AN. Work function and implications of doped poly(3,4-ethylenedioxythiophene)-co-poly(ethylene glycol). Appl Phys Lett 2006;88:152107.
[70] Pan CA, Ma TP. Work function of In_2O_3 film as determined from internal photoemission. Appl Phys Lett 1980;37:714–6.
[71] Kahn A. Fermi level, work function and vacuum level. Mater Horiz 2016;3:7–10.
[72] Wang JC, Karmakar RS, Lu YJ, Huang CY, Wei KC. Characterization of piezoresistive PEDOT:PSS pressure sensors with inter-digitated and cross-point electrode structures. Sensors 2015;15:818–31.